SUPPLEMENTARY MATERIALS

Reduced Temperature Sensitivity of Maximum Latewood Density Formation in High-Elevation Corsican Pines under Recent Warming

Philipp Römer, Claudia Hartl, Lea Schneider, Achim Bräuning, Sonja Szymczak, Frédéric Huneau, Sébastien Lebre, Frederick Reinig, Ulf Büntgen and Jan Esper

Table S1. MXD site chronology characteristics.

Code	Site [elevation]	Radii	Period	MSL	Rbar	EPS	AC1	AMXD
Asc	**Asco** [1600 m a.s.l.]	19	1360–2016	543	0.34	0.90	0.33	0.83
Tar	**Tartagine** [1450 m a.s.l.]	20	1636–2016	282	0.29	0.91	0.44	0.95
Sor	**Col de Sorba** [1400 m a.s.l.]	30	1622–1980	211	0.36	0.94	0.26	0.94

Period: Start and end dates when replication ≥5 radii. MSL: mean segment length [years]. Rbar: mean inter-series correlation. EPS: Expressed Population Signal. AC1: first-order autocorrelation. AMXD: average MXD [g/cm³].

Table S2. MXD composite chronology characteristics.

Chronology	Radii	Period	MSL	Rbar	EPS	AC1	AMXD
COR$_{RCS}$	69	1360–2016	325	0.23	0.91	0.44	0.92
ABC400	69	1361–2016	247	0.27	0.93	0.38	0.93
ABC300	69	1361–1988	200	0.27	0.93	0.37	0.94
ABC200	66	1365–1980	141	0.27	0.90	0.35	0.95

Period: Start and end dates when replication ≥5 radii. MSL: mean segment length [years]. Rbar: mean inter-series correlation. EPS: Expressed Population Signal. AC1: first-order autocorrelation. AMXD: average MXD [g/cm³].
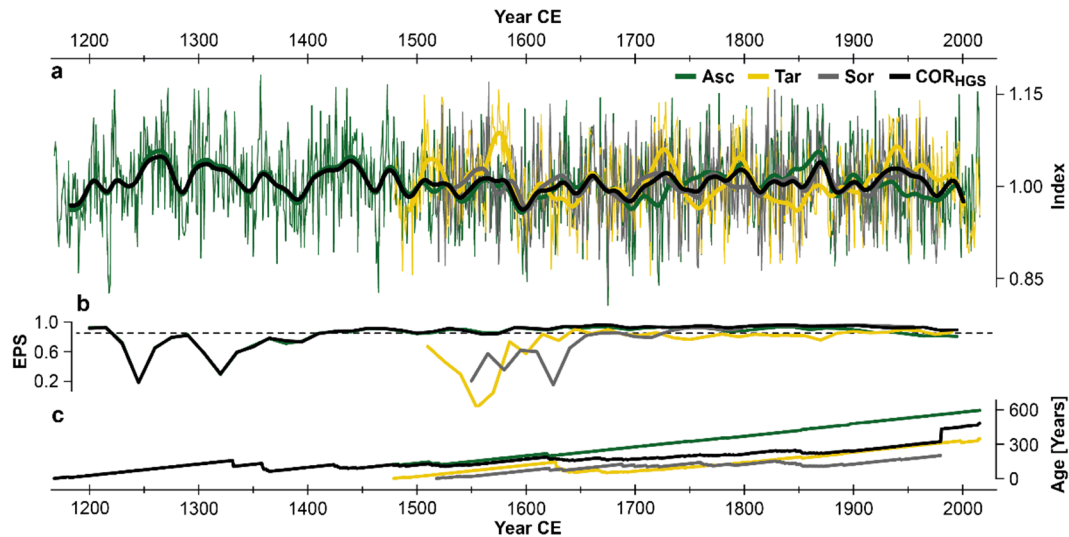

Figure S1. Effects of merging site measurements. **(a)** Hugershoff-detrended MXD composite (*COR$_{HGS}$*) and site chronologies (*Asc*, *Tar*, *Sor*) (thin curves) shown together with their 31-year smoothing splines (bold curves), **(b)** their Expressed Population Signal (EPS) computed for 30-year segments with a 15-year overlap and **(c)** their mean tree age curves.
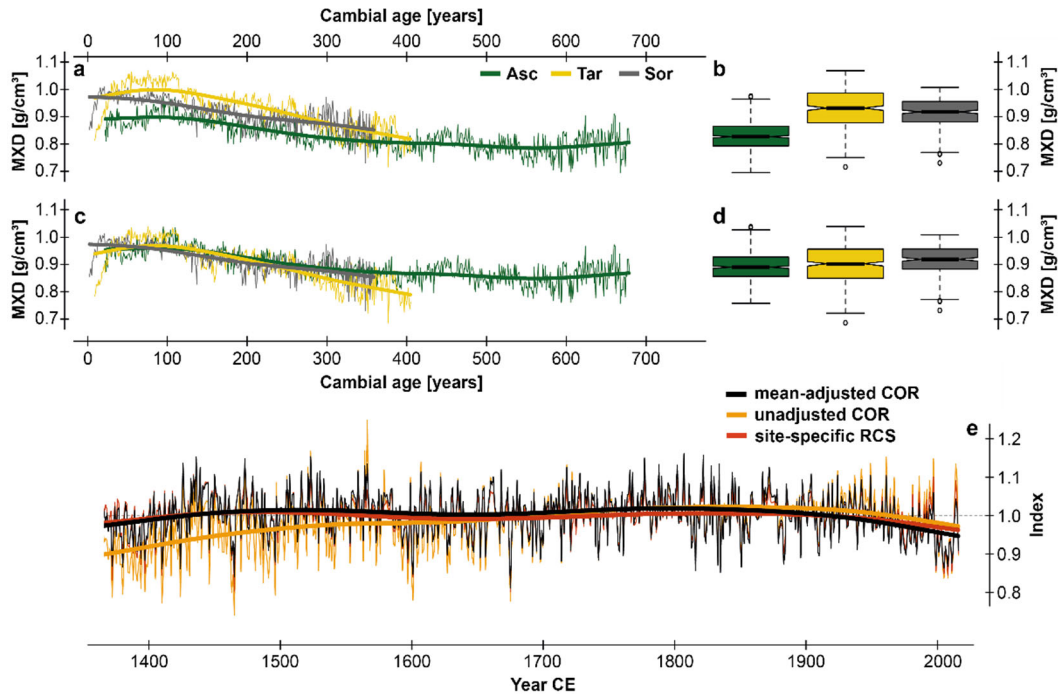
Figure S2: Effects of mean adjustment. Regional curves (thin curves) shown together with their 300-year splines (bold curves) and boxplots displaying growth rates of the site-specific MXD data **(a–b)** before mean-adjustment and **(c–d)** after mean-adjustment. **(e)** *COR* chronologies (thin curves) and their 300-year splines (bold curves) after applying RCS to the mean-adjusted data (black), RCS to the unadjusted data (orange) and RCS to the site-specific data before merging (red). Start and end dates were set to *n* ≥5 series. Note the considerably lower indices of the unadjusted chronology version before ~1600 CE (caused by the dominance of higher elevated trees from *Asc*).
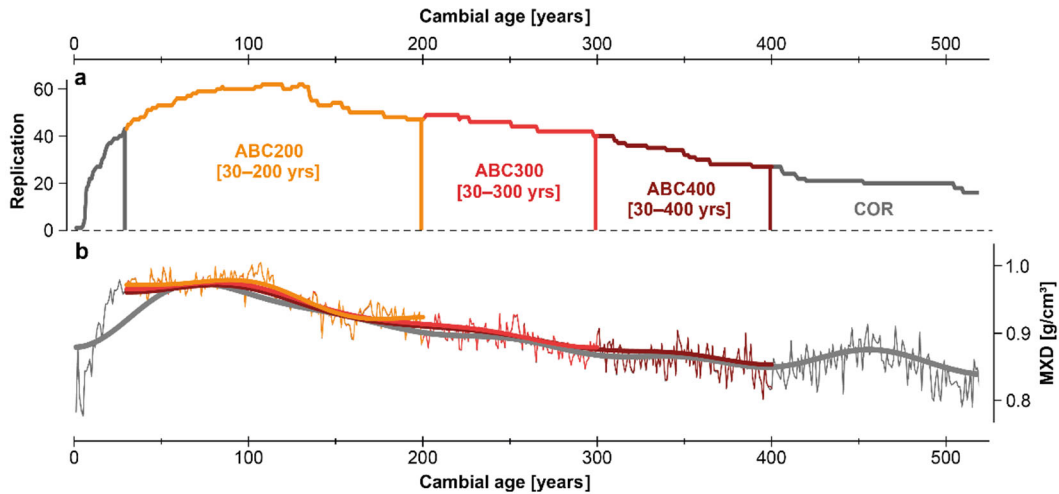

Figure S3. Sample replication and regional curves of the composite MXD data. **(a)** Replication curves of age-aligned rings highlighting the data sections: *ABC200* contains rings from 30–200 years, *ABC300* from 30–300 years and *ABC400* from 30–400 years. Rings younger than 30 years and older than 400 years are only included in *COR*. **(b)** The regional curves of the chronologies (light) shown together with their 100-year low pass filters (bold). Pith offset estimates are considered. Note the Hugershoff-shaped age-trend in *COR*.
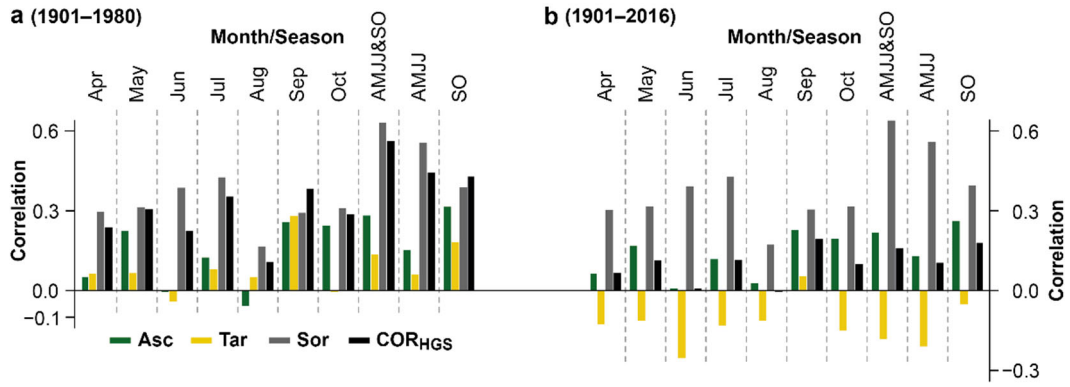
Figure S4. Temperature signal estimation using CRU TS4.04 data. Correlations between the Hugershoff-detrended chronologies and monthly and seasonal temperatures from **(a)** 1901–1980 and **(b)** 1901–2016 CE. Note that *Sor* ends in 1980 CE.
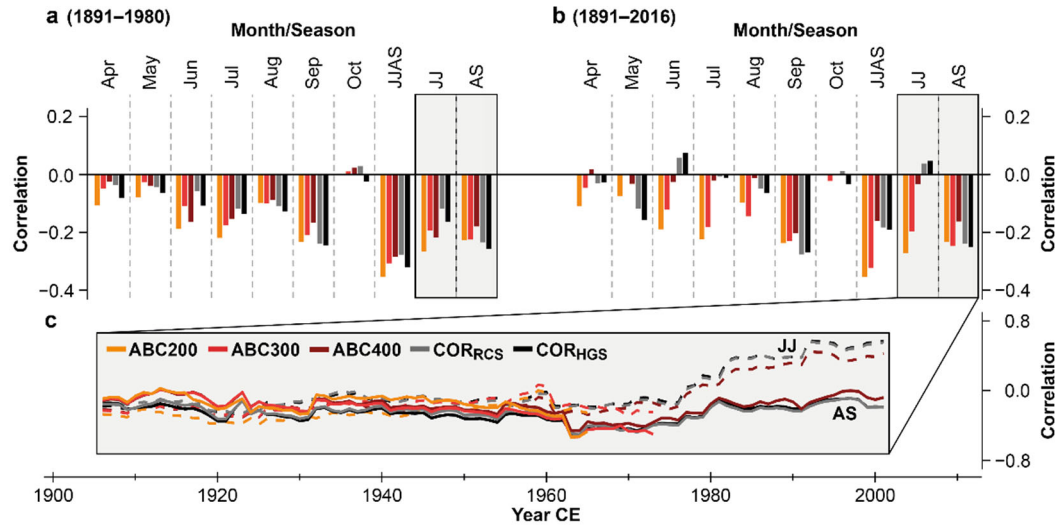

Figure S5. Precipitation signal estimation using GPCC v2020 data. Correlations between the MXD composite chronologies and monthly and seasonal precipitation totals from **(a)** 1891–1980 and **(b)** 1891–2016 CE. Note that *ABC200* and *ABC300* end in 1980 and 1988 CE, respectively. **(c)** The 31-year running correlations between the chronologies and June–July (JJ) and August–September (AS) precipitation totals.